Nanoscale

Using Post-synthetic Ligand Modification to Imprint Chirality onto the Electronic States of Cesium Lead Bromide (CsPbBr3) Perovskite Nanoparticles

Journal:	*Nanoscale*
Manuscript ID	NR-ART-07-2021-004274.R1
Article Type:	Paper
Date Submitted by the Author:	07-Aug-2021
Complete List of Authors:	Debnath, Gouranga; University of Pittsburgh, Department of Chemistry Georgieva, Zheni; University of Pittsburgh, Department of Chemistry Bloom, Brian; U Pittsburgh, Tan, Susheng; University of Pittsburgh, Petersen Institute of Nanoscience and Engineering Waldeck, David; University of Pittsburgh, Department of Chemistry

Using Post-synthetic Ligand Modification to Imprint Chirality onto the Electronic States of Cesium Lead Bromide ($CsPbBr_3$) Perovskite Nanoparticles

Gouranga H. Debnath,[1] Zheni N. Georgieva,[1] Brian P. Bloom,[1] Susheng Tan[2,3] and David H. Waldeck[1,3,*]

[1]Department of Chemistry, University of Pittsburgh, Pittsburgh, Pennsylvania 15260, United States

[2]Department of Electrical and Computer Engineering, University of Pittsburgh, Pittsburgh, Pennsylvania 15261, United States

[3]Petersen Institute of NanoScience and Engineering, University of Pittsburgh, Pittsburgh, Pennsylvania 15261, United States

E-mail: dave@pitt.edu

* To whom correspondence should be addressed.

Keywords: Perovskites, Chirality, Nanoparticles, Ligand Modification

---

Abstract: This study presents a post-synthetic ligand modification strategy for the generation of chiroptically active, blue emitting $CsPbBr_3$ nanoparticles (NPs); an expansion to the library of 3D chiral perovskite nanomaterials. Addition of [R- and S-] 1-phenylethylamine, 1-(1-naphthyl)ethylamine, or 2-aminooctane to the synthesized $CsPbBr_3$ NPs is shown to induce Cotton effects in the NP first exciton transition, suggestive of a successful electronic coupling between the chiral ligands and the NPs. The availability of these chiral $CsPbBr_3$ NPs thrusts them into the forefront of perovskite nanomaterials for examining the implications of the chiral induced spin selectivity (CISS) effect and other applications in spintronics.

Introduction: Synthetic strategies to generate metal halide perovskite semiconductor nanomaterials has grown exponentially over the past six years,[1] largely driven by their promising optoelectronic properties which include emission tunability over the entire visible spectral region (through modulation in halide composition and quantum confinement effects);[2, 3] high defect tolerance;[4] near unity fluorescence quantum yields (in cases);[5] low exciton binding energy, and high charge carrier mobility.[6] These properties have brought them to the forefront of applications in lasers,[7] light emitting diodes (LEDs),[8, 9] and photovoltaics,[10] among others. Of particular interest here are the recent developments in chiral perovskites and their general implications for the chiral induced spin selectivity (CISS) effect[11-15] which have led to demonstrations of spin polarized charge transport,[16-18] spin dependent photovoltaic and photogalvanic responses in optoelectronic devices,[19] and as sources for generating circularly polarized light.[20] In 2006 Billing and coworkers[21] introduced the possibility of incorporating chiral molecules in 1D or 2D hybrid organic-inorganic perovskites but it was not until 2017 when reports on the synthesis of chiroptically active hybrid organic-inorganic 2D metal halide perovskite thin films, pioneered by Moon and coworkers,[22] became available. The chiroptical activity was proposed to stem from chiral crystalline structures arising from twisted perovskite unit cells.[22] In 2018 we reported the synthesis of colloidal methylammonium lead bromide nanoplatelets[23] (NPLs) that exhibit both quantum confinement effects and chiroptical activity. The origin of the chiroptical activity was attributed to the electronic coupling of the chiral ligand shell and the NPLs. In comparison to the significant number of reports on chiral films and nanoplatelets, reports on 3D chiral perovskite nanomaterials are much less common. Duan and coworkers[24] reported the direct synthesis of chiral α-octylamine modified cesium lead bromide ($CsPbBr_3$) nanoparticles (NPs) that display circular dichroism and circularly polarized luminescence; they attributed the chiro-optical properties to

asymmetric distortions of the surface perovskite lattice induced by the chiral α-octylamine. A number of recent reviews are available and provide a more comprehensive introduction to the development and applications of chiral perovskites.[25-28]

An alternate strategy to the commonly deployed direct synthetic route for synthesizing chiral perovskites is post-synthetic modification of achiral perovskite NPs. The first report on such post-synthetic ligand exchange discussed the generation R and S-1,2-diaminocyclohexane (DACH) capped $CsPb(I/Br)_3$ NPs from their achiral counterparts;[29] however, the chiroptical response was centered around the ligand-perovskite charge transfer band with no signatures evident near the perovskite excitonic absorption maximum. Later, Liu and coworkers[30] co-assembled achiral cesium lead halide ($CsPbX_3$, X = Cl, Br, I) NPs with chiral lipid gelators to demonstrate circularly polarized luminescence from $CsPbX_3$ NPs. A report by Luther and coworkers[31] discusses the role of mixed achiral (oleylamine) and chiral (R-2-octylamine) ligands during synthesis followed by a post-synthetic ligand treatment by R/S-methylbenzyl ammonium bromide to produce circularly polarized luminescence from formamidium lead bromide ($FAPbBr_3$) NPs. Scheme 1 shows a post-synthetic ligand modification strategy that leads to the generation of chiral $CsPbBr_3$ NPs, starting from their achiral counterparts. This work demonstrates (i) a synthetic procedure to generate ultra-small, strongly quantum confined $CsPbBr_3$ NPs and (ii) a room temperature post-synthetic ligand modification strategy that imprints chirality onto the electronic states of $CsPbBr_3$ NPs and generates robust CD signatures centered on the NP excitonic transition - using chiral ligands like R- and S-1-phenylethylamine (R- and S-PEA), R- and S-2-aminooctane (R- and S-OcAm) and R- and S-1-(1-naphthyl)ethylamine (R- and S-NEA).

The CD signal intensity (in mdeg) and dissymmetry factors (in $\Delta A/A$) reported in this study is among the highest when compared to the available literature on chiral perovskite NPs

synthesized via ligand exchange.[29-31] While the ligand exchange strategy presented here follows the spirit of those used for typical II-VI semiconductors nanomaterials,[32] the intrinsically labile perovskite framework and the dynamic surface ligand composition present a different set of synthetic challenges for obtaining chiral $CsPbBr_3$ NPs that can sustain their chiroptical responses over time. Additionally, the post-synthetic approach is unique in that it allows one to monitor the chiral imprinting on the perovskite NPs before and after ligand addition, without having to account for the unwanted introduction of synthetic heterogeneity[33] which can play a role in modulating chiroptical responses[34]. Also, as shown in Scheme 1 unique chiral perovskite NPs can be generated from a large batch of achiral NPs by simply changing the identity of the chiral ligand during ligand exchange without having to depend on individual separate syntheses, thereby saving time and effort; a challenge one faces when using a direct synthetic strategy to generate chiral perovskite NPs with different ligand identity.

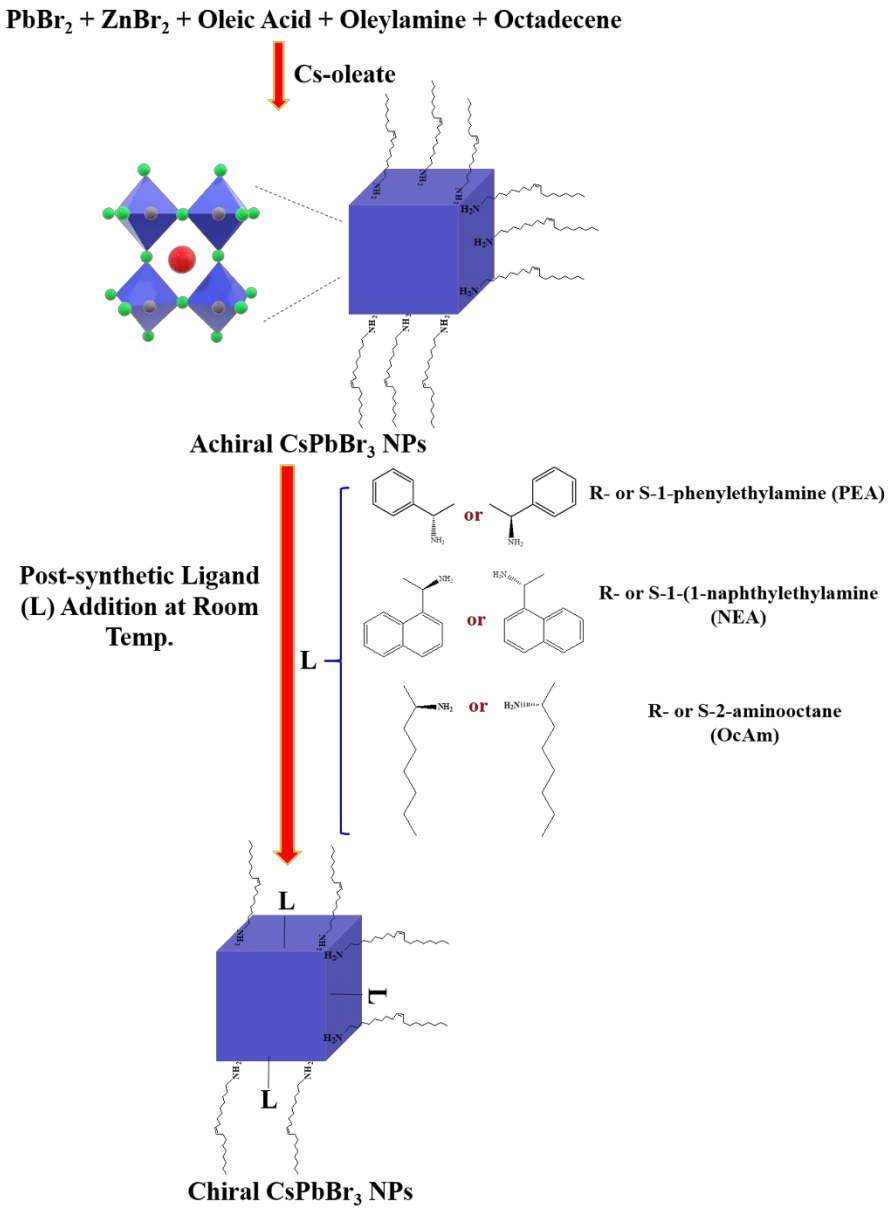

Scheme 1. Representation of the room temperature post-synthetic ligand modification leading to the generation of chiral $CsPbBr_3$ NPs from their achiral counterparts is shown.

Results and Discussion: $CsPbBr_3$ NPs were synthesized using previously published methods with modifications; see experimental section for details. Figure 1a shows the UV-visible absorption spectrum, and Figure 1b shows the emission spectrum of the synthesized $CsPbBr_3$ NPs (blue solid line) with absorption and emission maxima at 428 nm and 434 nm, respectively. Note that the currently available reports of blue emitting $CsPbBr_3$ nanomaterials in the literature emit

significantly to the red of 434 nm, in the 450-465 nm.[35-37] The high degree of quantum confinement for the NPs, and subsequent blue shift of the emission, reported here was achieved by having excess [Br^-] during the synthesis; a technique known to induce size focusing of $CsPbBr_3$ NPs (see experimental section for more details). Additional confirmation of this observation comes from electron microscopy studies (*vide infra*). A larger quantum confinement is believed also to provide larger electronic coupling between chiral ligands and the confined carriers' wavefunctions as reported by Markovich and coworkers for the size dependent chiroptical activity in chiral CdSe and CdS quantum dots.[38] The post-synthetic addition of R-PEA (black dashed line) and S-PEA (red solid line) to the $CsPbBr_3$ NPs modestly shifts the absorption (430 nm) and emission (436 nm) maxima to lower energies accompanied by the attenuation of higher excitonic transitions; see Figure 1. These observations, along with a gradual red shift in the absorption maximum of $CsPbBr_3$ NPs as a function R- and S-PEA concentration is shown in Figure S1 and its implications on the NP dimension is discussed later. The inherent defect tolerance of the perovskites[4] prevents any significant emission line broadening, which contrasts with the defect mediated broad emission bands that are often encountered while synthesizing chiral cadmium chalcogenide NPs.[39] The relative quantum yield of the $CsPbBr_3$ and R-/S-PEA-$CsPbBr_3$ NPs are 45% and 42% respectively; similar to reports by others for $CsPbBr_3$ NPs.[40] The lowering in the quantum yield for the R- and S-PEA-$CsPbBr_3$ NPs can be correlated to the reorganization of surface capping ligands and the introduction of associated non-radiative decay channels.[41] The changes in the average lifetime $\langle\tau\rangle$ from 5.85 ± 0.23 ns for the $CsPbBr_3$ NPs[40] to 3.0 ± 0.3 ns for the R-/S-PEA-$CsPbBr_3$ NPs further support this explanation (See Figure S2 and Table S1).

The retention of the emission line shape and the quantum yield of the R- and S-PEA-$CsPbBr_3$ NPs is an important outcome because a stable emission signature for chiral perovskite

NPs is a prerequisite to gauge their efficiency as circularly polarized luminophores.[24, 30] The spectroscopic and chiroptical properties of chiral 3D confined perovskite QDs and 2D NPLs have undergone significant evaluation.[25, 42] When compared to the chiral perovskite QDs, the design criteria of chiral NPLs must be studied further to overcome their stability issues. For example, a recent report by Tisdale and coworkers on n = 2 MAPbBr NPLs (absorption maximum = 434 nm; emission maximum = 437 nm; quantum yields = 3.5% to 6.8%), discusses their propensity to undergo degradation and further transformation into n = 3 or n = 4 structures on exposure to UV light.[43] This is reflected by a significant decrease in the intensity and broadening of their emission spectra (with emergence of new peaks centered at 455 and 474 nm).[43] A fundamental understanding of the efficiency of chiral imprinting/CD signatures in these assemblies of perovskite nanomaterials will require the establishment of detailed understanding of the effect of ligand identity[44], crystal structure,[34] and ligand concentration[45, 46] on the chiral imprinting for perovskite QDs and NPL building blocks.

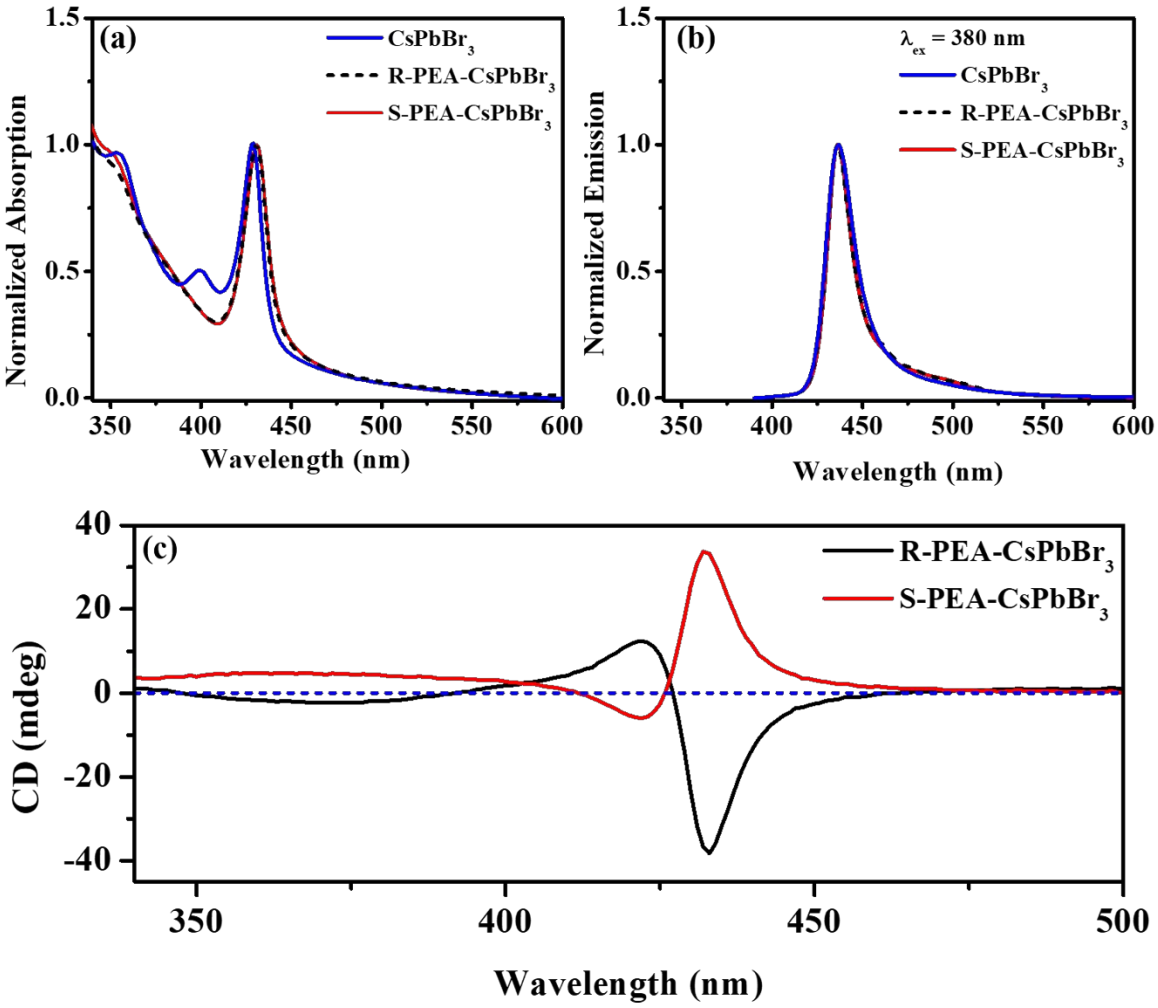

Figure 1. (a) Normalized absorption, (b) emission and (c) circular dichroism spectra of the $CsPbBr_3$, R- and S-PEA-$CsPbBr_3$ NPs in toluene are shown. The PEA concentration in the NP dispersion was maintained at 10mM for spectra in panels a-b and at 20 mM for panel c.

Circular dichroism (CD) spectra of the R-(black) and S-PEA-$CsPbBr_3$ NPs (red) in Figure 1c show mirror image profiles with R-PEA-$CsPbBr_3$ NPs displaying positive to negative Cotton effects and S-PEA-$CsPbBr_3$ NPs negative to positive Cotton effects near the absorption maximum, with increasing wavelength. The R- and S-PEA ligands, not on the surface of the NPs, display CD signals at wavelengths below 280 nm (see Figure S3). The strong overlap between the R- and S-PEA-$CsPbBr_3$ NP first excitonic transition with the bisignate CD spectral features (circa 400-460

nm) demonstrates the successful chiral imprinting of the R- and S-PEA onto the $CsPbBr_3$ NP electronic structure.[23]

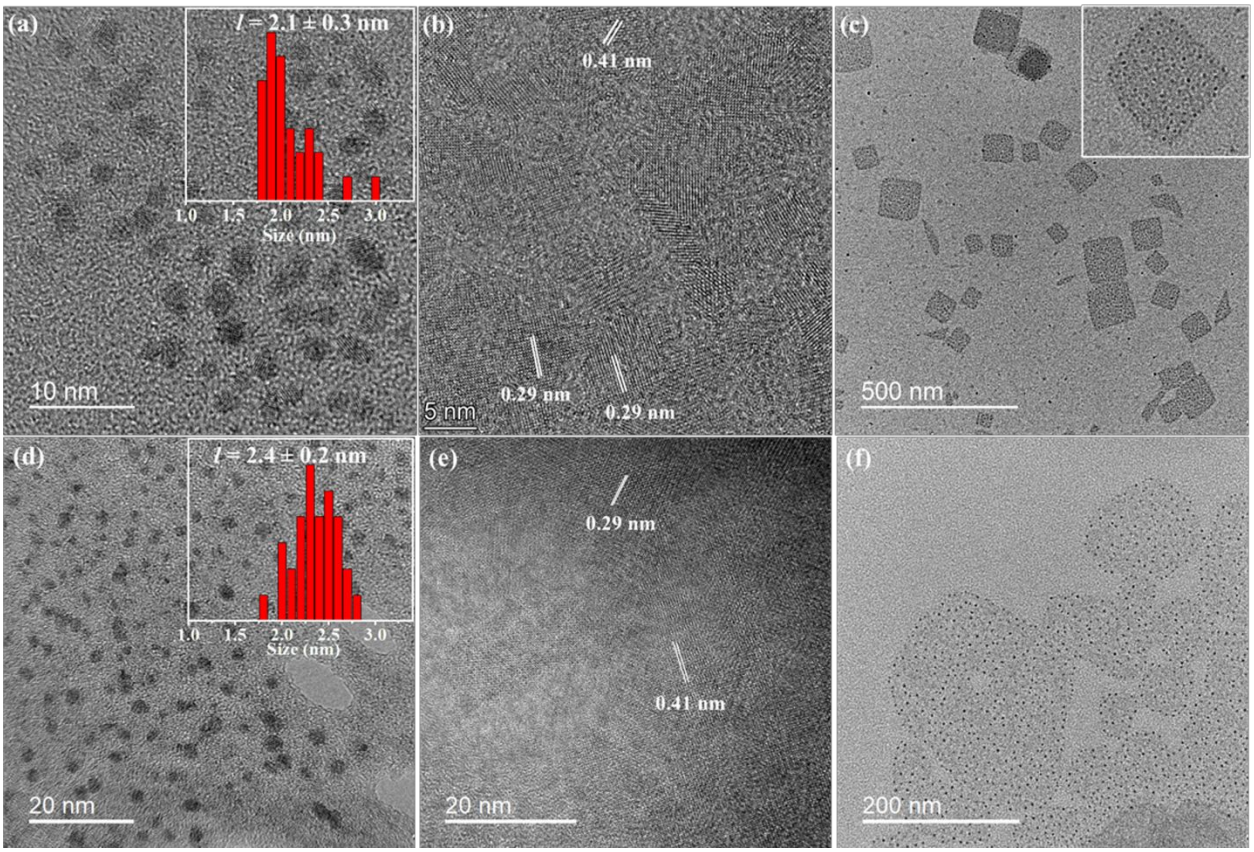

Figure 2. (a-c) TEM images of $CsPbBr_3$ NPs and their size distribution along with high resolution (HR) images and superstructured assemblies are shown. TEM, size distribution, HRTEM and superstructured images of PEA-$CsPbBr_3$ NPs are shown in panels (d-f, [PEA] = 10 mM in NP dispersion).

The transmission electron microscopy (TEM) images of the $CsPbBr_3$ NPs are shown in Figure 2 (a-c). The $CsPbBr_3$ NPs have quasi-cubic shapes with an average particle size of 2.1 ± 0.3 nm (panel a). This narrow particle size distribution is attributed to size focusing during synthesis; which was realized by maintaining a Br/Pb precursor ratio of ~20:1 and a growth time of three minutes at 85 ℃ (for details see experimental section). The lowest accessible $CsPbBr_3$ NP dimension reported (using an excess [Br^-]) stands at 3.7 nm with an excitonic absorption

maximum centered around 455-460 nm.[47] Note that the absence of excess [Br^-] at the mentioned synthetic conditions is known to produce non-emissive Cs_4PbBr_6 NPs.[47]

The high resolution TEM image (Figure 2b) of the $CsPbBr_3$ NPs shows lattice spacings of 0.29 and 0.41 nm which is consistent with the (220) and (020) planes of the orthorhombic $CsPbBr_3$.[48] Additional confirmation of this claim manifests in the powder XRD patterns of the $CsPbBr_3$ NPs (see Figure S4) with distinct peaks at 2θ = 13.2°, 15.2°, 21.6°, 30.7° and 34.5° corresponding to the (101), (110), (020), (220) and (130) planes of orthorhombic $CsPbBr_3$ crystal structure (PDF: 01-072-7929).[40, 48] The $CsPbBr_3$ NPs can also assemble into cube-like superstructures with domains spanning tens to hundreds of nanometers in length, see Figure 2c and is consistent with reports by Son and coworkers.[47]

The red shift in the first excitonic transition of $CsPbBr_3$ NPs upon ligand modification to R- and S-PEA-$CsPbBr_3$ NPs (see Figures 1 and S1) coincides with an increase in NP size. The TEM images indicate that the average size of the NPs increase from 2.1 ± 0.3 nm for the achiral $CsPbBr_3$ (Figure 2 a-c) to 2.4 ± 0.2 nm (Figure 2 d-f) with 10 mM PEA in the NP dispersion. The increase in NP size as a function of PEA concentration likely arises during the PEA induced restructuring of the oleylamine/oleic acid ligand shell. The subsequent destabilization of the ligand shell in the $CsPbBr_3$ NPs and the intrinsically labile perovskite framework allows the ~ 2 nm NPs to coalesce and is argued to attenuate the higher excitonic absorption transitions (see Figure 1). Changes in capping ligand concentration and solvent polarity have been shown to greatly affect the $CsPbX_3$ NP morphology leading to a wide gamut of shapes in the form of large cubes, wires, and rods through the oriented attachment of initially formed cubic seeds.[36] The identical d-spacings of 0.29 and 0.41 nm for the PEA-$CsPbBr_3$ NPs along with their assembly into

superstructures, much like the achiral $CsPbBr_3$ NPs, indicate the retention of the orthorhombic crystal phases.

X-ray photoelectron spectroscopy was used to further compare the $CsPbBr_3$ and R-PEA-$CsPbBr_3$ NPs. Figure S5 shows that the Cs 3d, Pb 4f, and Br 3d spectra do not change upon ligand modification and are in agreement with other reported values.[49, 50] Differences arise in the N1s and C1s spectra however.

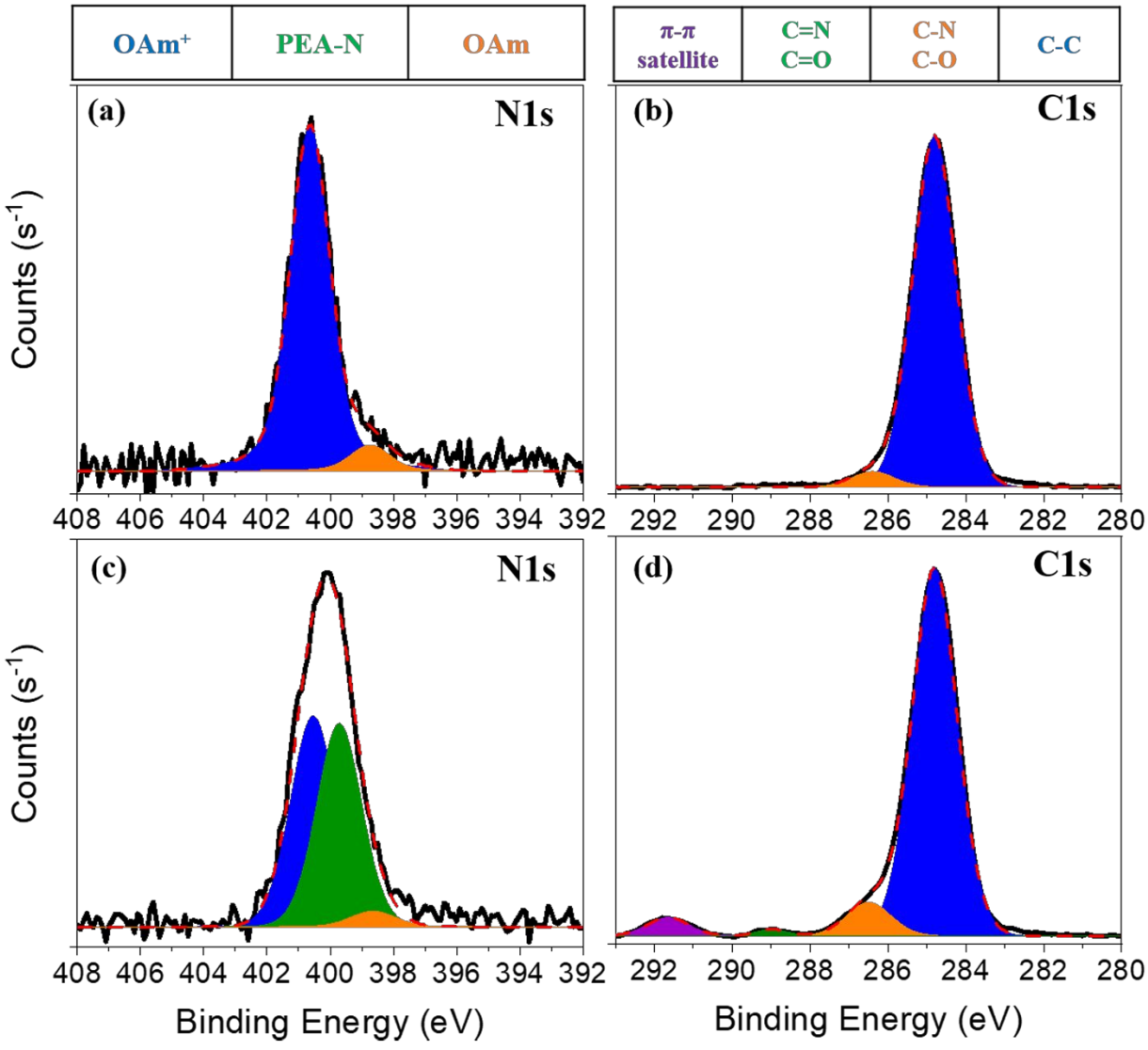

Figure 3. N1s and C1s X-ray photoelectron spectra of the $CsPbBr_3$ NPs (a,b) along with those of the R-PEA-$CsPbBr_3$ NPs (c, d) are shown.

The N1s spectrum (black) for the $CsPbBr_3$ NPs (Figure 3a) is fit to a sum of two peaks centered at 398.7 eV (orange) and 400.6 eV (blue) and correspond to oleylammonium (OAm^+) and oleylamine (OAm) respectively.[51] The full-width-at-half-maximum (FWHM) of the envelope marked by a red dashed line was found to be 1.7 eV. In contrast, the envelope for the N1s spectrum for the R-PEA-$CsPbBr_3$ NPs (Figure 3c) shows a distinct broadening with an increase in FWHM to 2.2 eV. The spectrum was fit to a sum of three peaks at 398.7 eV (orange), 399.8 eV (green) and 400.6 eV (blue) and the emergence of the new peak at 399.8 eV is attributed to contributions from the nitrogen on the PEA ligand.

The C1s spectrum (black) for the $CsPbBr_3$ NPs (Figure 3b) is fit to a sum of two peaks at 286.4 eV (blue) and 284.8 eV (orange) which originate from the C–C and C–N/C–O components of OAm/OA respectively.[52] The C1s spectrum of the R-PEA-$CsPbBr_3$ NPs (Figure 3d) shows two additional peaks, barring the C–C and C–N/C–O components, at 289 eV (green) and 291.7 eV (purple) and they are attributed to C=N/C=O and π–π satellite components[52] of the PEAs, respectively. These observations further corroborate the presence of the PEA ligands without detrimental changes to the integrity of the $CsPbBr_3$ NPs. Additional XPS spectra of the R-NEA-$CsPbBr_3$ NPs and R-OcAm-$CsPbBr_3$ NPs are shown in Fig S6-S7 and exhibit a similar behavior to that described for the PEAs.

To further confirm the presence of the chiral ligands on the surface of the NPs ^1H NMR spectroscopy was performed on purified $CsPbBr_3$, R- and S-PEA-$CsPbBr_3$ NPs; see Figures S8 and S9. Because ligand binding to the NP surface is known to induce signal broadening and attenuation, dissolution of the $CsPbBr_3$ NPs in DMSO-d6 was performed.[53] NMR spectral analysis of the solutions generated from the $CsPbBr_3$ dissolution showed resonances [assignment]

corresponding to CH_3[6], CH_2 [3], H_2C–HC= [4 and 5 respectively], NH_2 [α], α-CH_2 [1 for oleic acid, β for oleylamine], β-CH_2 [2]. These resonances overlap with the ^{1}H NMR of oleic acid (OA, pink) and oleylamine (OAm, red) and confirm the presence of the ligands in the $CsPbBr_3$ NPs; in agreement with the literature reports.[54, 55] For the R-PEA-$CsPbBr_3$ in DMSO-d6 (blue), additional phenyl [Z], methylene [Y], and methyl [X] resonances are present and further validate that the ligand shell comprises both PEA and OA/OAm.[23, 31] Proof of principle experiments illustrating the attenuation of bound ligands is shown in Figure S10 where NMR spectra of the purified R-PEA-$CsPbBr_3$ NPs in toluene-d8 show attenuated Z, Y, and X resonances, compared to the dissolution of the same material in DMSO-d6. The weak signal intensity of the PEA resonances in toluene-d8 indicates that the ^{1}H NMR in the DMSO-d6 solution does not arise from the unbound/unpurified ligands. Additional NMR spectra R- and S-NEA-$CsPbBr_3$ NPs and their corresponding ligands are presented in Figure S11. These experiments further illustrate the success of the ligand modification strategy.

The progression of the CD response in R- and S-PEA-$CsPbBr_3$ NPs as a function of ligand concentration is presented in Figure 4 (a, b, d). The spectra are presented as ΔA/A, the difference in absorptivity normalized to the absorbance at 430 nm.[23] The general trend is similar for both R- and S-PEA and they show a gradual increase in ΔA/A as a function of PEA concentration that is used in the ligand modification. We anticipate a saturation in the available ligand binding sites on the NP surface to dictate the observed trend. The increase in ΔA/A is accompanied by a gradual red shift in the CD minima (maxima) for the R-PEA-$CsPbBr_3$ (S-PEA-$CsPbBr_3$) NPs and results from an increase in the NP size as evident by the TEM results. A similar observation has been noted by Gun'ko and coworkers on D-/L-cysteine (Cys) capped CdSe/CdS NPs, which shows the evolution of CD intensity with Cys concentration.[46]

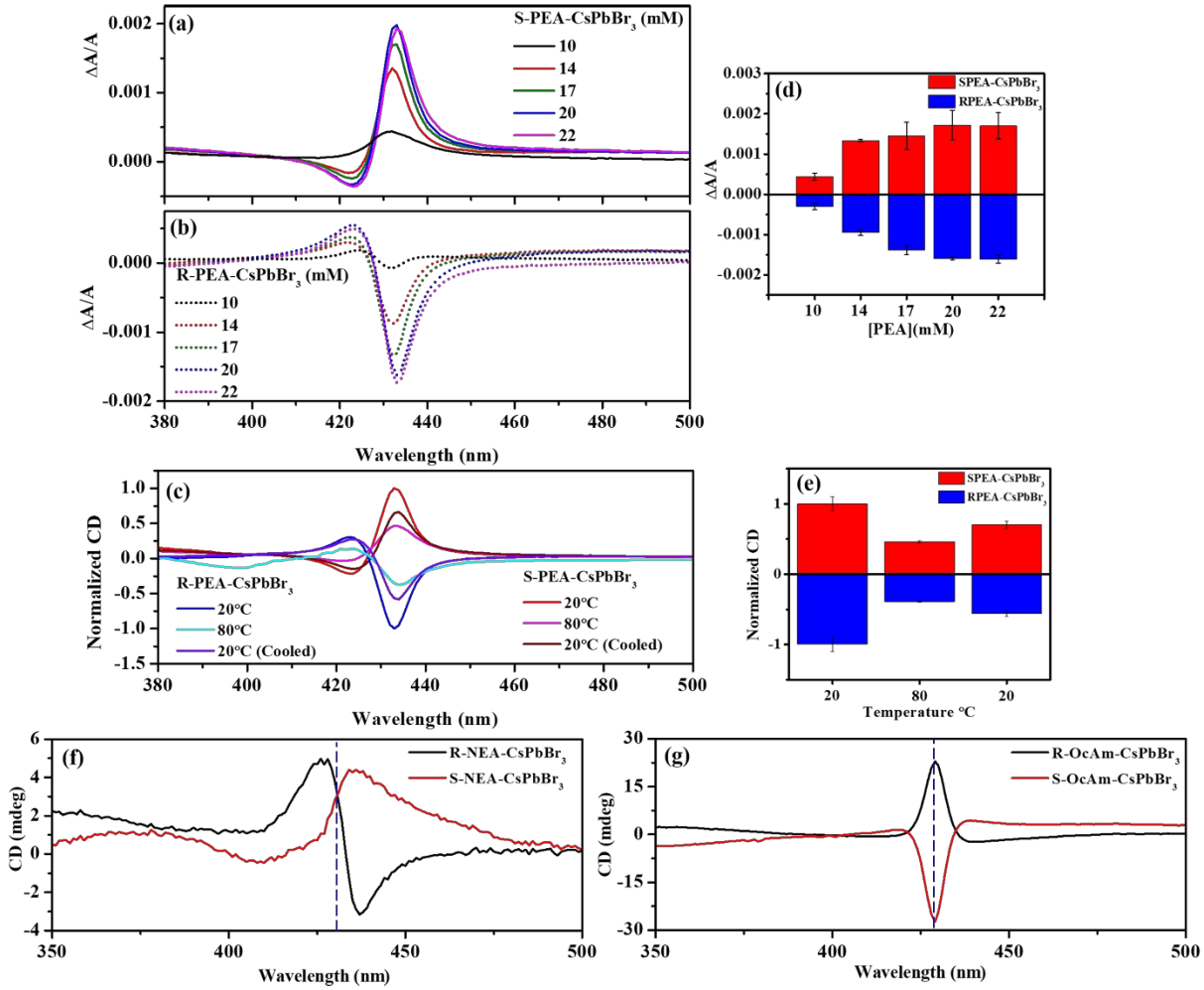

Figure 4. (a,b,d) Shows the concentration dependent evolution of CD strengths in R- and S-PEA $CsPbBr_3$ NPs represented in values of ΔA/A. (c, e) Shows the effect of thermal cycling on the CD intensities of R-and S-PEA-$CsPbBr_3$ NPs ([PEA] = 20 mM in NP dispersion). (f,g) Shows the CD spectra of R- and S-NEA-$CsPbBr_3$ NPs ([NEA = 30 mM in NP dispersion) and R- and S-OcAm-$CsPbBr_3$ NPs ([OcAm] = 11 mM in NP dispersion) highlighting the generality of the post-synthetic ligand modification. The peak position of the first exciton in each case is marked with a blue dashed line. The NPs were dispersed in toluene.

The effect of thermal cycling on the CD intensities was also evaluated for R- and S-PEA-$CsPbBr_3$ NPs; see Figure 4 (c, e). For both enantiomers, a reduction in CD intensity from the initial value is observed as the temperature is increased from 20 °C to 80 °C; the CD intensity is reduced to 39% for R- and 46% for S-PEA-$CsPBr_3$ NPs. Cycling the temperature back to 20°C

led to a partial, but incomplete, recovery of the CD intensity to ~70% of the original value; see Figure 4e. Ligand binding in $CsPbBr_3$ NPs has been shown to be a highly dynamic process with the existence of a fast exchange between the free and bound forms.[54] A temperature mediated shift in the PEA adsorption-desorption equilibrium, with an increase in temperature generating a greater population of unbound/loosely bound ligands is the most plausible explanation for the observed temperature dependence.

To demonstrate the effectiveness and generality of the post-synthetic ligand modification strategy, the study was extended to include chiral 2-aminooctane (R- and S-OcAm) and 1-(1-naphthyl)ethylamine (R-and S-NEA) modified $CsPbBr_3$ NPs; see Figure 4(f-g). Similar to the case for R- and S-PEA-$CsPbBr_3$ NPs, both the R- and S-OcAm-$CsPbBr_3$ NPs and R- and S-NEA-$CsPbBr_3$ NPs show near-mirror image CD signals in the region of the NP absorption maximum, thereby indicating the successful imprinting of chirality. The CD spectra of the R- and S-OcAm and R- and S-NEA ligands in solution, i.e., without the NPs are shown in Figures S12 and S13, respectively. The absorption spectra of the R- and S-NEA-$CsPbBr_3$ NPs and R- and S-OcAm-$CsPbBr_3$ NPs are shown in Figure S14 and are consistent with the perovskite excitonic absorption feature seen for R- and S-PEA-$CsPbBr_3$ NPs. The dissymmetry factors for the R and S- PEA-$CsPbBr_3$ NPs (Figure 4) and R- and S-OcAm-$CsPbBr_3$ NPs (see Fig S15) are an order of magnitude higher than the ones reported for chiral 2-octylamine capped $CsPbBr_3$ NPs (with an excitonic absorption maximum at 508 nm and an average particle size of 20 nm)[24] and highlights the importance of a strongly quantum confined system which provides a larger electronic coupling between chiral ligands and the confined carriers' wavefunctions, thereby affecting CD strengths. Finally, the evolution of the CD signals in chiral $CsPbBr_3$ NPs as a function of time is evaluated. R- and S-OcAm-$CsPbBr_3$ NPs were chosen particularly because of their similarity to oleylamine,

which forms an integral part of the ligand shell for the achiral $CsPbBr_3$ NPs. The progression of the CD response as a function of ligand incubation time is shown in Figure S15 for R- and S-OcAm-$CsPbBr_3$ NPs. Although the CD signals decrease with time following the degradation of the NPs, as evidenced from the decrease in their absorption spectra (see Fig S16), there is an observable CD response even after 168 hour of ligand incubation.

Conclusions

This study demonstrates a post-synthetic ligand modification strategy for synthesizing chiral 3D $CsPbBr_3$ NPs. Highly quantum confined $CsPbBr_3$ NPs were synthesized by tuning the Br/Pb ratio during synthesis and the post-synthetic addition of R- and S-PEA to the $CsPbBr_3$ NP solution was used to induce chiroptical activity. The chiroptical activity is argued to originate from the electronic coupling of the ligands to the quantum confined $CsPbBr_3$ NPs. When compared to the achiral $CsPbBr_3$ NPs, TEM revealed a modest increase in NP size upon increasing PEA concentration. A concentration dependent evolution of CD signals was also observed. Thermal cycling was also shown to modulate the CD strengths in the R- and S-PEA-$CsPbBr_3$ NPs and was attributed to the temperature dependent binding strength of the chiral ligands. The post-synthetic strategy was then extended to generate chiral R- and S-OcAm-$CsPbBr_3$ NPs and R- and S-NEA-$CsPbBr_3$ NPs. The methods presented in this work further develop strategies for creating 3D chiral perovskites which may enable new opportunities for their application in spintronics and optoelectronics.

Experimental Details

Materials: Cesium carbonate (Cs_2CO_3, 99.9% trace metals basis), lead (II) bromide ($PbBr_2$, 99.999% trace metals basis), zinc (II) bromide ($ZnBr_2$, 99.999% trace metals basis), oleic acid (OA, technical grade, 90%), oleylamine (OAm, technical grade, 70%), octadecene (ODE, 90%),

R(+)-1-phenylethylamine (R-PEA, ≥99%), S(-)-1-phenylethylamine (S-PEA, ≥99%), R(+)-1-(1-naphthyl)ethylamine (R-NEA, ≥99%), S(-)-1-(1-naphthyl)ethylamine (S-NEA, ≥99%) and coumarin 153 (C153, 98%) were purchased from Sigma Aldrich. R-(-)-2-aminooctane (99+%) and S-(+)-2-aminooctane (99+%) were purchased from Alfa Aesar. Dimethyl sulfoxide (DMSO)-d6 was purchased from Cambridge Isotope Laboratories Inc. Toluene-d8 was purchased from Acros Organics. Toluene, acetone and tert-butanol were purchased from Fisher. All chemicals were used without further purification.

Synthesis of $CsPbBr_3$ NPs: $CsPbBr_3$ NPs were synthesized according to the reports by Son and coworkers with modifications.[47] For a typical synthesis 0.2 g Cs_2CO_3, 0.68 ml OA and 10 ml ODE were loaded onto a 50 ml three neck round bottomed (RB) flask and flushed with argon for 1 hour at 120 ℃. The reaction was then sealed in an argon atmosphere and the temperature was raised to 140 ℃ for the complete dissolution of Cs_2CO_3 to form Cs-oleate. The reaction temperature was then maintained at 120 ℃ to prevent precipitation of Cs-oleate.

In another 50 ml three neck RB flask 80 mg $PbBr_2$, 600 mg $ZnBr_2$, 2 ml OA, 2 ml OAm and 5 ml ODE were flushed with argon for 45 minutes at 120 ℃ after which the reaction was sealed in the argon atmosphere and heated at 120 ℃ for an additional 45 minutes. The temperature was then decreased to 85 ℃ and after equilibration, 0.8 ml Cs-oleate was rapidly injected. The reaction was quenched after 180 seconds by cooling the flask in an ice bath.

Next, 2 ml of the crude mixture was dispersed in 5 ml of toluene and then centrifuged at 6500 rpm for 15 minutes to remove any unreacted precursors. The supernatant was collected, left unagitated for a few hours and then concentrated further by bubbling in argon and centrifuged at 11000 rpm at 4 ℃ for 30 minutes to collect the purified nanoparticles. A few drops of acetone or tert-butanol was sometimes added to facilitate complete precipitation.

Post-synthetic Ligand Modification of Achiral $CsPbBr_3$ NPs by R- or S-OcAm and R- or S-NEA: $CsPbBr_3$ NPs dispersed in toluene were prepared with an optical density (O.D.) ≈ 1.0 at the first excitonic transition (428-430 nm). To the dispersions, R- or S-PEA was added so that the final concentration of the R- or S-PEA in solution ranged from 10-22 mM and incubated overnight at room temperature before further characterization. A similar approach was used for the modification of $CsPbBr_3$ NPs by R- or S-OcAm and R- or S-NEA.

UV-Visible Absorption and Emission Spectroscopy: UV-Visible absorption spectra were collected on an Agilent 8453 spectrometer. Steady-state emission spectra were collected using a Horiba Jobin Yvon Fluoromax 3 fluorescence spectrometer with an integration time of 1 sec and a spectral resolution of 2 nm. The relative emission quantum yields of the samples (Φ_x) were calculated with respect to coumarin 153 (C153) dissolved in methanol ($\Phi_r = 0.42$)[56] using equation 1.

$$\frac{\Phi_x}{\Phi_r} = \frac{A_r(\lambda_r)\, I_{ex}(\lambda_r)\, \eta_x^2 \int_0^\infty I_{em,x}(\bar{\upsilon})\, d\bar{\upsilon}}{A_x(\lambda_x)\, I_{ex}(\lambda_x)\, \eta_r^2 \int_0^\infty I_{em,r}(\bar{\upsilon})\, d\bar{\upsilon}} \quad (1)$$

where the subscripts x and r stand for sample and reference respectively, A is the absorbance at excitation wavelength (λ), I_{ex} is the intensity of the excitation light at the same wavelength, η is the refractive index (η = 1.496 for toluene and 1.327 for methanol) and $I_{em}(\bar{\upsilon})$ is the emission intensity as a function of wavenumber ($\bar{\upsilon}$). The experiments were performed at room temperature.

Time-resolved Luminescence Spectroscopy: The time-resolved emission decay profiles of the $CsPbBr_3$ and R- and S-PEA-$CsPbBr_3$ NPs were collected using the time-correlated single photon counting (TCSPC) method with a PicoHarp 300 TCSPC module (PicoQuant GmbH). The samples were excited using a picosecond diode laser at 378 nm (PiL037SM) with a repetition rate of 1MHz and the emission was collected at the magic angle. The full-width-at-half-maxima (FWHM) of the

instrument response function (IRF) was ≤ 96 ps. The decays were fitted using an iterative reconvolution method with the fluorescence analysis software (FAST) from Edinburgh Instruments.

Circular Dichroism (CD) Spectroscopy: CD spectra were collected with an OLIS DSM 17 CD spectrometer. NP dispersions in toluene with an O.D. ≈ 1.0 at the first excitonic transition were typically used for measurements along with an integration time of 3 sec and a spectral resolution of 1 nm. The spectra are reported in units of mdeg (degrees of ellipticity) and ΔA/A (difference in absorptivity normalized to absorption). The reported spectra are background subtracted with an achiral $CsPbBr_3$ NP acting as a blank. All spectra were acquired at 20 ℃. For temperature dependent CD experiments, the samples were cycled from 20 to 80 ℃.

Transmission Electron Microscope (TEM) Imaging: The TEM images were acquired using a JEOL JEM-2100F and a Thermo Fisher Scientific Titan Themis 200 aberration corrected TEM operated at an acceleration potential of 200 kV. The samples were prepared by drop-casting a 10 µl NP dispersion in toluene onto a Cu TEM grid with ultra-thin carbon supporting film and dried in air.

X-ray Diffraction (XRD): Powder XRD patterns were collected from a Bruker D8 Discover XRD instrument equipped with a PSD (LYNXEYE) detector operated with an X-ray generator voltage and current of 40 kV and 40 mA respectively along with a Cu Kα source (λ = 1.54187 Å). Concentrated NP dispersions were drop-cast on a clean glass substrate and then dried before acquiring the spectra at room temperature. Data analysis was performed on the EVA and HighScore XRD analysis software.

X-ray Photoelectron Spectroscopy (XPS): XPS spectra were collected using a Thermo Fisher Scientific ESCALAB 250 Xi. Samples were prepared by drop-casting a concentrated NP

dispersion in toluene on clean glass substrates and dried. Each spectrum was referenced to adventitious carbon (C 1s 284.8 eV).

^{1}H Nuclear Magnetic Resonance (NMR) Spectroscopy: ^{1}H NMR spectra were obtained using a Bruker Advance 400 MHz spectrometer. The spectra were calibrated to the residual solvent peak (DMSO-d6, 2.50 ppm). To prepare NP samples for NMR, purified suspensions of NPs in toluene were centrifuged into a pellet, then dried under Ar flow and stored in a vacuum desiccator. DMSO-d6 (~1 g) was added to the dried NPs and mixed until complete digestion occurred, as indicated by the formation of a clear solution.

Associated Content

Electronic Supplementary Information

UV-vis absorption, Emission Decay, CD, XRD, XPS, NMR spectra and Table (PDF)

Conflict of Interest

The authors declare no competing financial interests.

Acknowledgments

The authors acknowledge U.S. Department of Energy (Grant no. ER46430) for supporting this work.

References

1. J. Shamsi, A. S. Urban, M. Imran, L. De Trizio and L. Manna, *Chem. Rev.*, 2019, **119**, 3296-3348.
2. L. Protesescu, S. Yakunin, M. I. Bodnarchuk, F. Krieg, R. Caputo, C. H. Hendon, R. X. Yang, A. Walsh and M. V. Kovalenko, *Nano Lett.*, 2015, **15**, 3692-3696.
3. Q. A. Akkerman, V. D'Innocenzo, S. Accornero, A. Scarpellini, A. Petrozza, M. Prato and L. Manna, *J. Am. Chem. Soc.*, 2015, **137**, 10276-10281.
4. H. Huang, M. I. Bodnarchuk, S. V. Kershaw, M. V. Kovalenko and A. L. Rogach, *ACS Energy Lett.*, 2017, **2**, 2071-2083.
5. F. Di Stasio, S. Christodoulou, N. Huo and G. Konstantatos, *Chem. Mater.*, 2017, **29**, 7663-7667.
6. L. M. Herz, *Annu. Phys. Rev. Chem*, 2016, **67**, 65-89.
7. H. Dong, C. Zhang, X. Liu, J. Yao and Y. S. Zhao, *Chem. Soc. Rev.*, 2020, **49**, 951-982.
8. Q. Van Le, H. W. Jang and S. Y. Kim, *Small Methods*, 2018, **2**, 1700419.

9. Y.-H. Kim, S. Kim, A. Kakekhani, J. Park, J. Park, Y.-H. Lee, H. Xu, S. Nagane, R. B. Wexler, D.-H. Kim, S. H. Jo, L. Martínez-Sarti, P. Tan, A. Sadhanala, G.-S. Park, Y.-W. Kim, B. Hu, H. J. Bolink, S. Yoo, R. H. Friend, A. M. Rappe and T.-W. Lee, *Nat. Photonics*, 2021, **15**, 148-155.
10. A. K. Jena, A. Kulkarni and T. Miyasaka, *Chem. Rev.*, 2019, **119**, 3036-3103.
11. R. Naaman and D. H. Waldeck, *J. Phys. Chem. Lett.*, 2012, **3**, 2178-2187.
12. R. Naaman and D. H. Waldeck, *Annu. Phys. Rev. Chem*, 2015, **66**, 263-281.
13. B. P. Bloom, Y. Lu, T. Metzger, S. Yochelis, Y. Paltiel, C. Fontanesi, S. Mishra, F. Tassinari, R. Naaman and D. H. Waldeck, *Phys. Chem. Chem. Phys.*, 2020, **22**, 21570-21582.
14. R. Naaman, Y. Paltiel and D. H. Waldeck, *J. Phys. Chem. Lett.*, 2020, **11**, 3660-3666.
15. R. Naaman, Y. Paltiel and D. H. Waldeck, *Acc. Chem. Res.*, 2020, **53**, 2659-2667.
16. H. Lu, C. Xiao, R. Song, T. Li, A. E. Maughan, A. Levin, R. Brunecky, J. J. Berry, D. B. Mitzi, V. Blum and M. C. Beard, *J. Am. Chem. Soc.*, 2020, **142**, 13030-13040.
17. H. Lu, J. Wang, C. Xiao, X. Pan, X. Chen, R. Brunecky, J. J. Berry, K. Zhu, M. C. Beard and Z. V. Vardeny, *Science Advances*, 2019, **5**, eaay0571.
18. Z. Huang, B. P. Bloom, X. Ni, Z. N. Georgieva, M. Marciesky, E. Vetter, F. Liu, D. H. Waldeck and D. Sun, *ACS Nano*, 2020, **14**, 10370-10375.
19. J. Wang, H. Lu, X. Pan, J. Xu, H. Liu, X. Liu, D. R. Khanal, M. F. Toney, M. C. Beard and Z. V. Vardeny, *ACS Nano*, 2021, **15**, 588-595.
20. Y.-H. Kim, Y. Zhai, H. Lu, X. Pan, C. Xiao, E. A. Gaulding, S. P. Harvey, J. J. Berry, Z. V. Vardeny, J. M. Luther and M. C. Beard, *Science*, 2021, **371**, 1129.
21. D. G. Billing and A. Lemmerer, *CrystEngComm*, 2006, **8**, 686-695.
22. J. Ahn, E. Lee, J. Tan, W. Yang, B. Kim and J. Moon, *Mater. Horiz.*, 2017, **4**, 851-856.
23. Z. N. Georgieva, B. P. Bloom, S. Ghosh and D. H. Waldeck, *Adv. Mater.*, 2018, **30**, 1800097.
24. W. Chen, S. Zhang, M. Zhou, T. Zhao, X. Qin, X. Liu, M. Liu and P. Duan, *J. Phys. Chem. Lett.*, 2019, **10**, 3290-3295.
25. Y. Dong, Y. Zhang, X. Li, Y. Feng, H. Zhang and J. Xu, *Small*, 2019, **15**, 1902237.
26. Y. Dang, X. Liu, B. Cao and X. Tao, *Matter*, 2021, **4**, 794-820.
27. G. Long, R. Sabatini, M. I. Saidaminov, G. Lakhwani, A. Rasmita, X. Liu, E. H. Sargent and W. Gao, *Nat. Rev. Mater.*, 2020, **5**, 423-439.
28. L. Xiao, T. An, L. Wang, X. Xu and H. Sun, *Nano Today*, 2020, **30**, 100824.
29. T. He, J. Li, X. Li, C. Ren, Y. Luo, F. Zhao, R. Chen, X. Lin and J. Zhang, *Appl. Phys. Lett.*, 2017, **111**, 151102.
30. Y. Shi, P. Duan, S. Huo, Y. Li and M. Liu, *Adv. Mater.*, 2018, **30**, 1705011.
31. Y.-H. Kim, Y. Zhai, E. A. Gaulding, S. N. Habisreutinger, T. Moot, B. A. Rosales, H. Lu, A. Hazarika, R. Brunecky, L. M. Wheeler, J. J. Berry, M. C. Beard and J. M. Luther, *ACS Nano*, 2020, **14**, 8816-8825.
32. U. Tohgha, K. Varga and M. Balaz, *Chem. Commun.*, 2013, **49**, 1844-1846.
33. B. H. Kim, J. Heo, S. Kim, C. F. Reboul, H. Chun, D. Kang, H. Bae, H. Hyun, J. Lim, H. Lee, B. Han, T. Hyeon, A. P. Alivisatos, P. Ercius, H. Elmlund and J. Park, *Science*, 2020, **368**, 60.
34. X. Gao, X. Zhang, L. Zhao, P. Huang, B. Han, J. Lv, X. Qiu, S.-H. Wei and Z. Tang, *Nano Lett.*, 2018, **18**, 6665-6671.
35. C. Bi, Z. Yao, X. Sun, X. Wei, J. Wang and J. Tian, *Adv. Mater.*, 2006722.

36. S. Seth and A. Samanta, *Sci. Rep.*, 2016, **6**, 37693.
37. J. Shamsi, D. Kubicki, M. Anaya, Y. Liu, K. Ji, K. Frohna, C. P. Grey, R. H. Friend and S. D. Stranks, *ACS Energy Lett.*, 2020, **5**, 1900-1907.
38. A. Ben Moshe, D. Szwarcman and G. Markovich, *ACS Nano*, 2011, **5**, 9034-9043.
39. M. P. Moloney, Y. K. Gun'ko and J. M. Kelly, *Chem. Commun.*, 2007, DOI: 10.1039/B704636G, 3900-3902.
40. G. Almeida, L. Goldoni, Q. Akkerman, Z. Dang, A. H. Khan, S. Marras, I. Moreels and L. Manna, *ACS Nano*, 2018, **12**, 1704-1711.
41. J. R. Lakowicz, *Principles of Fluorescence Spectroscopy*, Third edn.
42. S. Ma, J. Ahn and J. Moon, *Adv. Mater.*, 2021, 2005760.
43. S. K. Ha, C. M. Mauck and W. A. Tisdale, *Chem. Mater.*, 2019, **31**, 2486-2496.
44. U. Tohgha, K. K. Deol, A. G. Porter, S. G. Bartko, J. K. Choi, B. M. Leonard, K. Varga, J. Kubelka, G. Muller and M. Balaz, *ACS Nano*, 2013, **7**, 11094-11102.
45. J. Cheng, J. Hao, H. Liu, J. Li, J. Li, X. Zhu, X. Lin, K. Wang and T. He, *ACS Nano*, 2018, **12**, 5341-5350.
46. V. A. Kuznetsova, E. Mates-Torres, N. Prochukhan, M. Marcastel, F. Purcell-Milton, J. O'Brien, A. K. Visheratina, M. Martinez-Carmona, Y. Gromova, M. Garcia-Melchor and Y. K. Gun'ko, *ACS Nano*, 2019, **13**, 13560-13572.
47. Y. Dong, T. Qiao, D. Kim, D. Parobek, D. Rossi and D. H. Son, *Nano Lett.*, 2018, **18**, 3716-3722.
48. A. Kostopoulou, M. Sygletou, K. Brintakis, A. Lappas and E. Stratakis, *Nanoscale*, 2017, **9**, 18202-18207.
49. E. Rathore, K. Maji, D. Rao, B. Saha and K. Biswas, *J. Phys. Chem. Lett.*, 2020, **11**, 8002-8007.
50. Y. Wang, Y. Ren, S. Zhang, J. Wu, J. Song, X. Li, J. Xu, C. H. Sow, H. Zeng and H. Sun, *Commun. Phys.*, 2018, **1**, 96.
51. S. Shahriar, V. Castaneda, M. Martinez, A. K. Mishra, T. Akter, K. Schutt, J. A. Boscoboinik and D. Hodges, *Journal of Renewable and Sustainable Energy*, 2019, **11**, 053504.
52. P. Chen, Y. Bai, S. Wang, M. Lyu, J.-H. Yun and L. Wang, *Adv. Funct. Mater.*, 2018, **28**, 1706923.
53. Z. Hens and J. C. Martins, *Chem. Mater.*, 2013, **25**, 1211-1221.
54. J. De Roo, M. Ibáñez, P. Geiregat, G. Nedelcu, W. Walravens, J. Maes, J. C. Martins, I. Van Driessche, M. V. Kovalenko and Z. Hens, *ACS Nano*, 2016, **10**, 2071-2081.
55. T. Udayabhaskararao, L. Houben, H. Cohen, M. Menahem, I. Pinkas, L. Avram, T. Wolf, A. Teitelboim, M. Leskes, O. Yaffe, D. Oron and M. Kazes, *Chem. Mater.*, 2018, **30**, 84-93.
56. J. E. Lewis and M. Maroncelli, *Chem. Phys. Lett.*, 1998, **282**, 197-203.